APPENDIX 4.9.1
CALCULATION OF EFFECTIVE PROPERTIES FOR HOMOGENIZED FUEL ASSEMBLIES

Table of Contents

List of Tables

List of Figures

4.9.1 CALCULATION OF EFFECTIVE PROPERTIES FOR HOMOGENIZED FUEL ASSEMBLIES

This section presents the methodology and determines the bounding effective thermal conductivity, specific heat and density for the irradiated spent fuel assemblies (SFAs) for use in the thermal analysis of the EOS-37PTH and EOS-89BTH DSCs. The EOS-37PTH and EOS-89BTH DSC basket assemblies are made up of interlocking slotted plates to form an egg-crate type structure with a grid of 37 and 89 fuel compartments, respectively, that house the fuel assemblies (FAs).

The surface properties of the components that make up the fuel compartment, along with the properties of the FAs, are used to determine the effective thermal properties. Emissivities of 0.8 and 0.09 are used for the Zircaloy fuel cladding and the aluminum sections of the fuel compartment opening as noted in Section 4.2.1. The emissivity of [ ] steel surfaces used in the evaluation is also listed in Section 4.2.1. The thermal properties of irradiated uranium dioxide (UO_2) and the fuel cladding are listed in Table 4.9.1-1 and Table 4.9.1-2, respectively.

The following conservatisms and assumptions are considered in the calculation of effective properties for FAs in EOS-37PTH and EOS-89BTH DSCs:

- Convection heat transfer within fuel assembly is neglected.
- The radiative heat transfer between fuel pellets and fuel cladding is neglected.
- The backfill gas and fuel pellets are not included in the FA axial effective thermal conductivity calculation as required by NUREG-1536 [4.9.1-1].
- The backfill gas is conservatively not included in calculating the FA effective density and specific heat.
- The FA is centered within a fuel compartment which maximizes thermal resistance between the fuel assembly and the compartment wall.
- For the pressurized water reactor (PWR) fuel, the instrument tube is not included in the cross-section of WE14x14 FA model. Change of instrument tube to fuel rod increases the heat generation in the center of the FA and the maximum temperature of the FA, which results in lower effective thermal conductivity of the FA.

4.9.1.1 Effective Thermal Properties for PWR Spent Fuel Assemblies in EOS-37PTH DSC

The FAs considered for storage in the EOS-37PTH DSC, including the design data for each fuel assembly, are listed in Table 2-2 and Table 2-4. The FAs listed in Table 2-2 are previously studied in Section M.4.8 and Section P.4.8 of the Updated Final Safety Analysis Report (UFSAR) for the Standardized NUHOMS® System [4.9.1-2]. In addition to the FAs analyzed in Section M.4.8 and Section P.4.8 of the Standardized NUHOMS® System UFSAR, the EOS-37PTH DSC allows for the storage of certain European and Japanese FAs as shown in Table 2-4.

A comparison of the FA characteristics of the European and Japanese FAs from Table 2-4 to those previously analyzed in Table 2-2 shows that they are either identical or very similar as described below.

- Geometry of Doel 1 and 2 (assembly type 14x14) FA and Kansai (assembly type 14x14 Step I Type A) FA are identical or similar to WE14x14 FA. The active fuel length for Doel 1 and 2 is 96 inches, which is shorter than WE14x14 FA. The heat load for this FA will be adjusted as described in Section 4.9.1.3.
- Geometry of Tihange 1 (assembly type 15x15) FA and Kansai (assembly type 15x15 Step I Type A) FA are identical or similar to WE 15x15 FA.
- Geometry of Doel 3 and 4 (assembly type 17x17) FA, Tihange 2 (assembly type 17x17) FA, Tihange 3 (assembly type 17x17) fuel assembly, Kansai (assembly type 17x17 Step II) FA, ENRESA ASCO (assembly type 17x17) FA, and AM1000 (assembly type 17x17) FA are identical or similar to WE17x17 FA.

Since the European or Japanese FAs are identical or very similar to the assemblies presented in Table 2-2, the thermal properties for these FAs will be bounded by the properties of the corresponding assemblies from Table 2-2. Among the various FAs listed in Table 2-2, based on the study in Section P.4.8 of the Standardized NUHOMS® System UFSAR, the WE 14x14 FA has the bounding transverse effective conductivity, bounding axial effective conductivity, bounding effective density, and bounding effective specific heat.

Since the same FAs or their corresponding versions (European and Japanese fuel assemblies) are considered for storage within the EOS-37PTH DSC, the effective thermal properties for WE 14x14 are recomputed using the methodologies presented in Section M.4.8 and Section P.4.8 of the Standardized NUHOMS® System UFSAR using irradiated UO_2 properties and the EOS-37PTH DSC basket configuration shown in the drawings in Section 1.3.1.

The methodology to determine the axial conductivity is described in Section P.4.8.1.3 of the Standardized NUHOMS® System UFSAR [4.9.1-2] and is used in this evaluation based on the bounding FA and the properties described above. Similarly, the effective density and specific heat are determined based on the methodology presented in Section P.4.8.2 of the Standardized NUHOMS® System UFSAR, using the bounding FA and the properties described above.

Using the methodology presented in Appendix P, Section P.4.8.1.4 of the Standardized NUHOMS® System [4.9.1-2], a two-dimensional (2D) finite element model (FEM) of WE14x14 OFA FA is developed in ANSYS [4.9.1-3] to determine the transverse effective conductivity. The outer surfaces, representing the fuel compartment walls, are held at a constant temperature, and heat generating boundary condition is applied to the fuel pellets within the model. The models were run with a series of isothermal boundary conditions applied to the nodes representing the fuel compartment walls. The FEMs of WE14x14 OFA FA is shown in Figure 4.9.1-1. Figure 4.9.1-2 shows the heat generation rate and temperature boundary conditions.

The computed FA transverse and axial effective conductivities as functions of temperature for irradiated WE14x14 FA are listed in Table 4.9.1-3 and also summarized in Section 4.2.1. The effective specific heat and density for irradiated WE14x14 FA is shown is listed in Table 4.9.1-4 and also summarized in Section 4.2.1. The effective thermal conductivities for the FAs are also applicable for vacuum drying conditions since helium is used for water blowdown from the DSC.

4.9.1.2 Effective Thermal Properties for BWR Spent Fuel Assemblies in EOS-89BTH DSC

The FAs considered for storage in the EOS-89BTH DSC including the design data for each FA, are listed in Table 2-3 and Table 2-4. The FAs listed in Table 2-3 are previously studied in Section T.4.8 and Section Y.4.9 of the Standardized NUHOMS® System UFSAR[4.9.1-2], except for the GNF2 FA. However, the dimensions of GNF2 FA listed in Table 2-3 are very similar to the previously evaluated GE12/GE14 FAs from Section T.4.8 and Section Y.4.9 of the Standardized NUHOMS® System UFSAR. Therefore, the thermal properties for the GE12/GE14 FAs are also applicable to the GNF2 FA.

In addition to the FAs analyzed in Section T.4.8 and Section Y.4.9 of the Standardized NUHOMS® System UFSAR, the EOS-89BTH DSC allows for the storage of certain European and Japanese FAs as shown in Table 2-4. Since transient evaluations are not performed for the EOS-89BTH DSC in Sections 4.4, 4.5, and 4.6,only the effective transverse and axial conductivities are presented for the FAs allowed for storage in the EOS-89BTH DSC.

A comparison of the FA characteristics of the European and Japanese FAs from Table 2-4 to those previously analyzed in Table 2-3 shows that they are either identical or very similar as described below.

- Geometries of Japanese boiling water reactor (BWR) FA (assembly type 8x8 Step II) and Switzerland– KKL BWR 1/4 fuel assembly (assembly type 8x8) from Table 2-4 are similar to GE8 Type II FA (TN ID: 8x8-60/4) from Table 2-3.
- Geometry of Switzerland– KKL BWR 2/5/8 FA (assembly type 9x9) from Table 2-4 is similar to GE 11/13 FA (TN ID: 9x9-74/2) from Table 2-3.
- Geometry of Switzerland– KKL BWR 3/9/12/13 FA (assembly type 10x10) from Table 2-4 is similar to GE 12/14 FA (TN ID: 10x10-92/2) from Table 2-3.
- Geometry of Switzerland– KKL BWR 6 FA (assembly type 4x4x4) from Table 2-4 is identical or similar to SVEA-64 FA from Table 2-3.
- Geometries of Switzerland– KKL BWR 7/14 FA (assembly type 4x(5x5-1)), BWR 10/15 FA (assembly type 4x(5x5-3)/4x(5x5-1)) and BWR 11/16 FA (assembly type 4x(5x5-4)/4x(5x5-2)/4x(5x5-1)) from Table 2-4 are similar to SVEA-96 FA from Table 2-3.

Since the European or Japanese FAs are identical or very similar to the assemblies presented in Table 2-3, the thermal properties for theseFAs will be bounded by the properties of the corresponding assemblies from Table 2-3. Among the various FAs listed in Table 2-3, based on the study in Section T.4.8 and Section Y.4.9 of the Standardized NUHOMS® System UFSAR, the FANP 9x9-81 FA has the bounding transverse effective conductivity. Therefore, the transverse effective conductivities are recomputed using the methodologies presented in Section T.4.8 of the Standardized NUHOMS® System UFSAR using irradiated UO_2 properties and the EOS-89BTH DSC basket configuration shown in the drawings in Section 1.3.2.

Using the methodology presented in Section T.4.8.1.4 of the Standardized NUHOMS® System UFSAR, a 2D FEM of FANP 9x9-81 FA is developed in ANSYS [4.9.1-3] to determine the transverse effective conductivity. The outer surfaces, representing the fuel compartment walls, are held at a constant temperature, and heat generating boundary condition is applied to the fuel pellets within the model. The models were run with a series of isothermal boundary conditions applied to the nodes representing the fuel compartment walls. The FEMs FANP 9x9-81 FA is shown in Figure 4.9.1-3. Figure 4.9.1-4 shows the heat generation rate and temperature boundary conditions.

The methodology to determine the axial conductivity is described in Section T.4.8.1.3 of the Standardized NUHOMS® System [4.9.1-2] and is used in this evaluation for the various FAs listed in Table 2-3 and Table 2-4.

The computed bounding fuel assembly transverse and axial effective conductivities as functions of temperature for the various FAs allowed for storage in EOS-89BTH DSC are listed in Table 4.9.1-5 and also summarized in Section 4.2.1. The effective thermal conductivities determined for the bounding FAs are also applicable for vacuum drying conditions since helium is used for water blowdown from the DSC.

4.9.1.3 Scaling Factors for Short and Long Fuel Assemblies

The various heat load zone configuration (HLZCs) presented in Figure 1 of the Technical Specifications [4.9.1-6] for the EOS-37PTH DSC and Figure 2 of the Technical Specifications [4.9.1-6] for the EOS-89BTH DSC are evaluated in Sections 4.4, 4.5, and 4.6 at the maximum allowable heat loads for each HLZC, assuming that the FA has an active fuel length of 144 inches.

For FAs with active fuel length shorter than 144 inches, there is a possibility that the concentration of the heat generation in a smaller volume might result in a non-conservative temperature distribution. To ensure that the temperature distributions evaluated in Sections 4.4, 4.5, and 4.6 remain bounding, the maximum allowable heat load for FAs with active fuel length shorter than 144 inches should be determined as discussed below.

Since conduction with effective conductivities is the only heat transfer path considered in the EOS-37PTH and EOS-89BTH DSCs, the temperatures are directly proportional to the FA heat load and inversely proportional to the active fuel length and effective fuel conductivity. Therefore, the following equations are used to determine the heat load for FAs with active fuel length shorter than 144 inches in order to maintain the temperatures at the same level as those determined from the bounding FAs.

$$\left(\frac{q}{L_a\ k_{eff}}\right)_{Short\ FA} = \left(\frac{q}{L_a\ k_{eff}}\right)_{Bounding\ FA}$$

$$q_{Short\ FA} = q_{Bounding\ FA} \cdot SF,$$

$$SF = \frac{L_{a,Short\ FA}}{L_{a,Bounding\ FA}} \cdot \frac{k_{eff,Short\ FA}}{k_{eff,Bounding\ FA}}.$$

Where,

k_{eff} = Effective conductivity for FA,
q = Decay heat load per assembly defined for each loading zone,
L_a = Active fuel length,
SF = Scaling factor (SF) for short FAs.

The SF determined from the equation should be used to reduce the maximum heat load per FA in each loading zone of the HLZCs presented Figure 1 of the Technical Specifications [4.9.1-6] for the EOS-37PTH DSC and Figure 2 of the Technical Specifications [4.9.1-6] for the EOS-89BTH DSC.

In the above equation, the effective conductivities for the bounding FA are presented in Table 4.9.1-3 and Table 4.9.1-5 for the EOS-37PTH DSC and EOS-89BTH DSC, respectively. The effective conductivity for the shorter FA should be determined using the same approach presented in Sections 4.9.1.1 for the PWR FAs and Section 4.9.1.2 for the BWR FAs.

However, for FAs with active fuel length greater than 144 inches, no scaling is necessary and the maximum heat loads listed for each HLZC in Figure 1 of the Technical Specifications [4.9.1-6] for the EOS-37PTH DSC and Figure 2 of the Technical Specifications [4.9.1-6] for the EOS-89BTH DSC are applicable.

4.9.1.4 References

4.9.1-1 NUREG-1536, "Standard Review Plan for Spent Fuel Dry Cask Storage Systems at a General License Facility," Revision 1, U.S. Nuclear Regulatory Commission, July 2010.

4.9.1-2 AREVA Inc., "Updated Final Safety Analysis Report, Standardized NUHOMS® Horizontal Modular Storage System for Irradiated Nuclear Fuel, NUH-003," Revision 14, September 2014.

4.9.1-3 ANSYS Mechanical APDL, Version 10.0.

4.9.1-4 NUREG/CR-7024 (PNNL-19417), "Material Property Correlations: Comparisons between FRAPCON-3.4, FRAPTRAN 1.4, and MATPRO," U.S. Nuclear Regulatory Commission, March 2011.

4.9.1-5 Oak Ridge National Laboratory, RSIC Computer Code Collection, "SCALE, A Modular Code System for Performing Standardized Computer Analysis for Licensing Evaluation," NUREG/CR-0200, Rev. 6, Volume 3, Section M8 (ORNL/NUREG/CSD-2/V3/R6), Oak Ridge National Laboratory, Oak Ridge, Tennessee, May 2000.

4.9.1-6 Proposed CoC 1042 Appendix A, NUHOMS® EOS System Generic Technical Specifications, Amendment 0.

Table 4.9.1-1
Irradiated UO_2 Thermal Properties

T	Thermal Conductivity (Equation 2.3-9 of [4.9.1-4])	T	Specific Heat (Equation 2.2-1 of [4.9.1-4])	Density (95% of TD of [4.9.1-5])
°F	Btu/(hr-in-°F)	°F	Btu/(lb_m-°F)	lb_m/in^3
100	0.138	32	0.054	0.376
200	0.133	212	0.062	
300	0.128	392	0.067	
400	0.123	752	0.071	
500	0.119	1502	0.076	
600	0.116			
700	0.112			
800	0.109			
900	0.107			
1000	0.105			

Table 4.9.1-2
Fuel Cladding Thermal Properties

T	Thermal Conductivity (Equation 3.2-1 of [4.9.1-4])	T	Specific Heat (Table 3.1-1 of [4.9.1-4])	Density [4.9.1-5]
°F	Btu/(hr-in-°F)	°F	Btu/(lb_m-°F)	lb_m/in^3
100	0.618	80	0.067	0.237
200	0.655	260	0.072	
300	0.690	692	0.079	
400	0.723	1502	0.090	
500	0.756			
600	0.787			
700	0.819			
800	0.851			
900	0.883			
1000	0.916			

Table 4.9.1-3
Bounding Transverse and Axial Effective Thermal Conductivities of Fuel Assemblies in EOS-37PTH DSC

T	k_{eff}	T	k_{axl}
(°F)	Btu/(hr-in-°F)	(°F)	Btu/(hr-in-°F)
160	1.467E-02	200	4.606E-02
251	1.728E-02	300	4.852E-02
343	2.054E-02	400	5.084E-02
436	2.459E-02	500	5.316E-02
530	2.910E-02	600	5.534E-02
626	3.423E-02	800	5.984E-02
722	3.968E-02		
819	4.719E-02		
916	5.456E-02		
1014	6.236E-02		
1113	6.984E-02		
SI UNITS			
T	k_{eff}	T	k_{axl}
(°C)	W/(m-K)	(°C)	W/(m-K)
71	3.047E-01	93	0.957
121	3.589E-01	149	1.008
173	4.266E-01	204	1.056
224	5.107E-01	260	1.104
277	6.043E-01	316	1.149
330	7.110E-01	427	1.243
383	8.241E-01		
437	9.800E-01		
491	1.133E+00		
546	1.295E+00		
600	1.450E+00		

Table 4.9.1-4
Bounding Effective Specific Heat and Density of Fuel Assemblies in EOS-37PTH DSC

T	$C_{p\ eff}$	ρ_{eff}
(°F)	Btu/(lb_m-°F)	(lb_m/in^3)
80	0.0576	0.0968
260	0.0646	
692	0.0719	
1502	0.0779	
SI units		
T	$C_{p\ eff}$	ρ_{eff}
(°C)	kJ/(kg-K)	(kg/m^3)
27	0.2411	2679
127	0.2706	
367	0.3008	
817	0.3263	

Table 4.9.1-5
Bounding Transverse and Axial Effective Thermal Conductivities of Fuel Assemblies in EOS-89BTH DSC

T	k_{eff}	T	k_{axl}
(°F)	Btu/(hr-in-(°F)	(°F)	Btu/(hr-in-(°F)
124	0.0141	200	0.0427
220	0.0165	300	0.0450
317	0.0194	400	0.0472
415	0.0228	500	0.0493
513	0.0267	600	0.0514
611	0.0312	800	0.0555
709	0.0360		
808	0.0414		
907	0.0476		
1006	0.0541		
1106	0.0610		
SI UNITS			
T	k_{eff}	T	k_{axl}
(°C)	W/(m-K)	(°C)	W/(m-K)
51	2.918E-01	93	0.888
105	3.420E-01	149	0.935
159	4.023E-01	204	204
213	4.735E-01	260	1.024
267	5.547E-01	316	1.066
322	6.476E-01	427	1.153
376	7.486E-01		
431	8.595E-01		
486	9.875E-01		
541	1.123E+00		
596	1.266E+00		

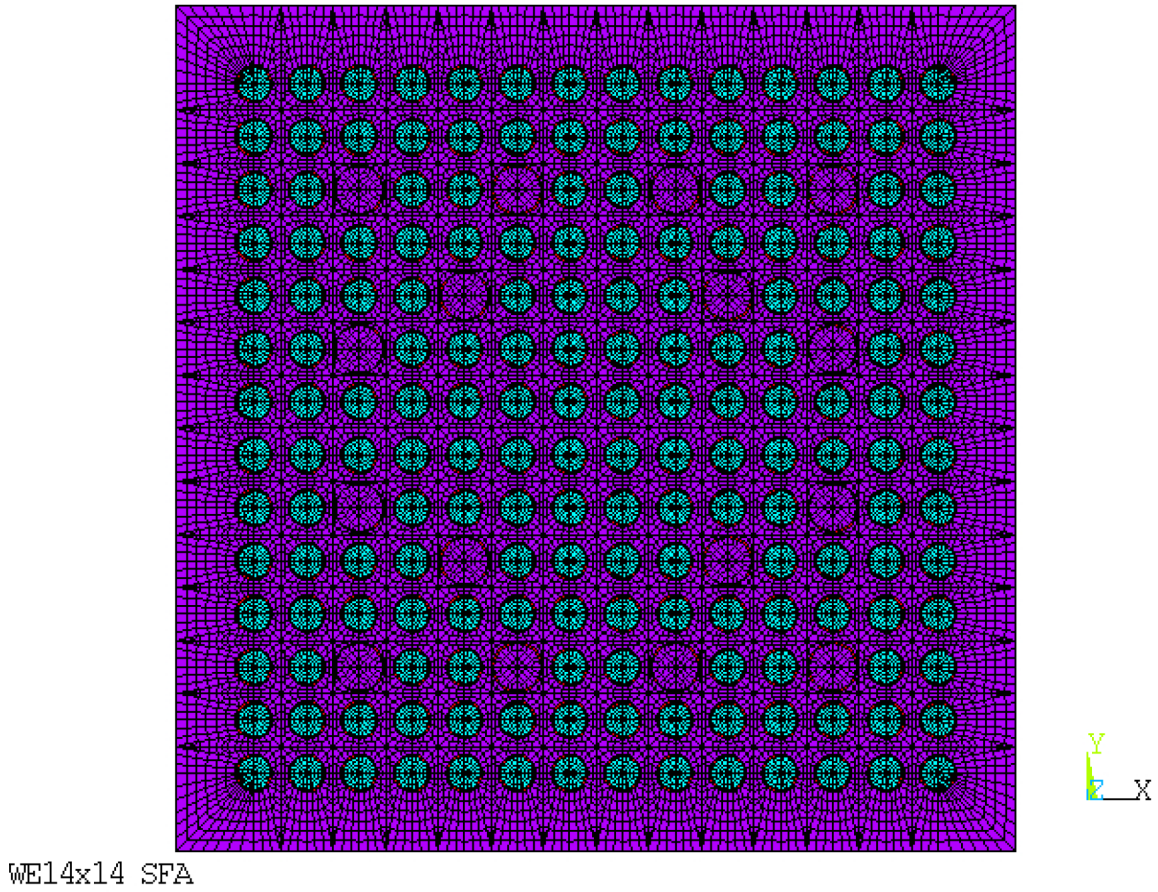

Figure 4.9.1-1
Finite Element Model of WE14x14 Fuel Assembly

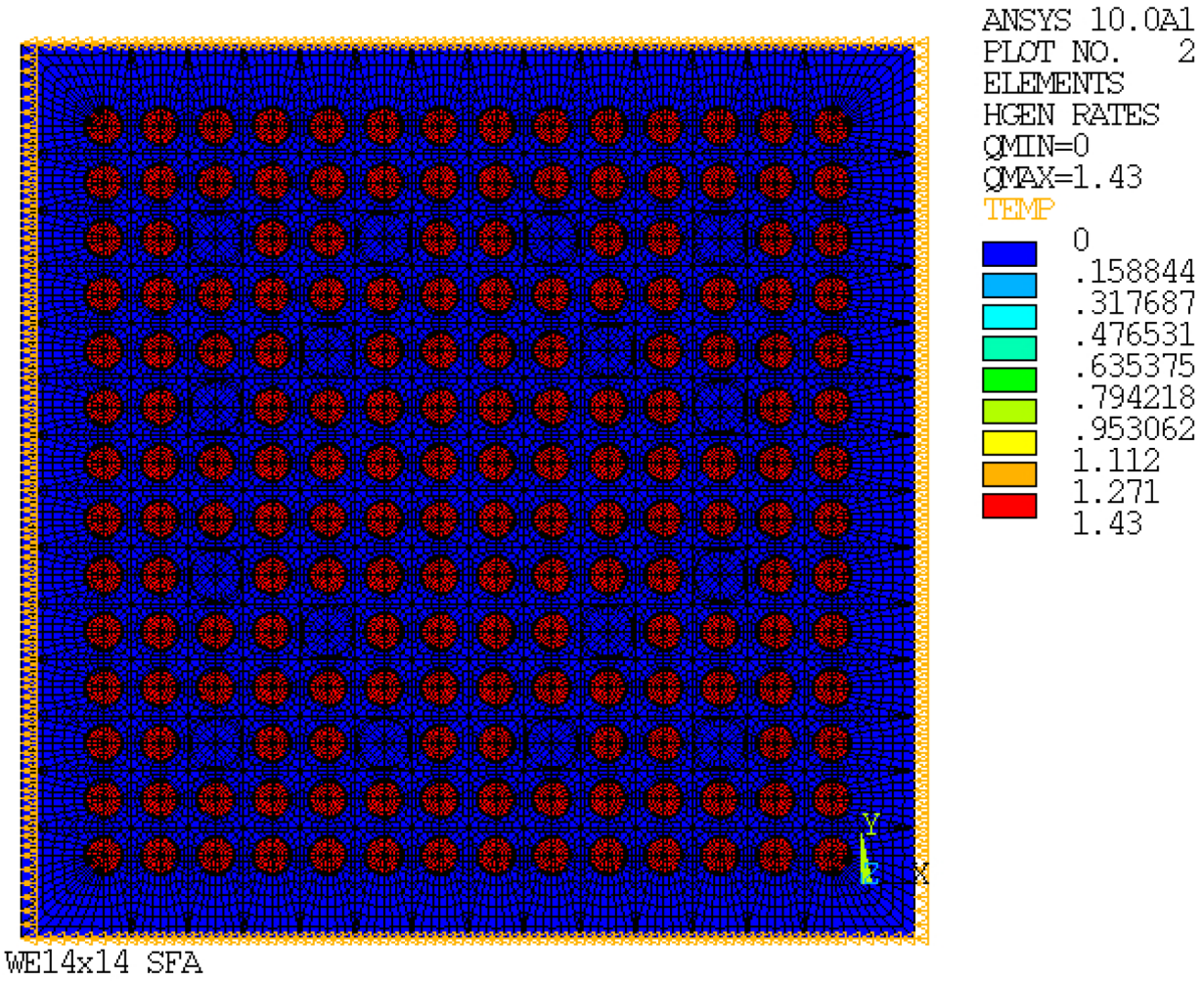

Figure 4.9.1-2
Heat Generation Rate and Temperature Boundary Conditions for WE14x14 Fuel Assembly

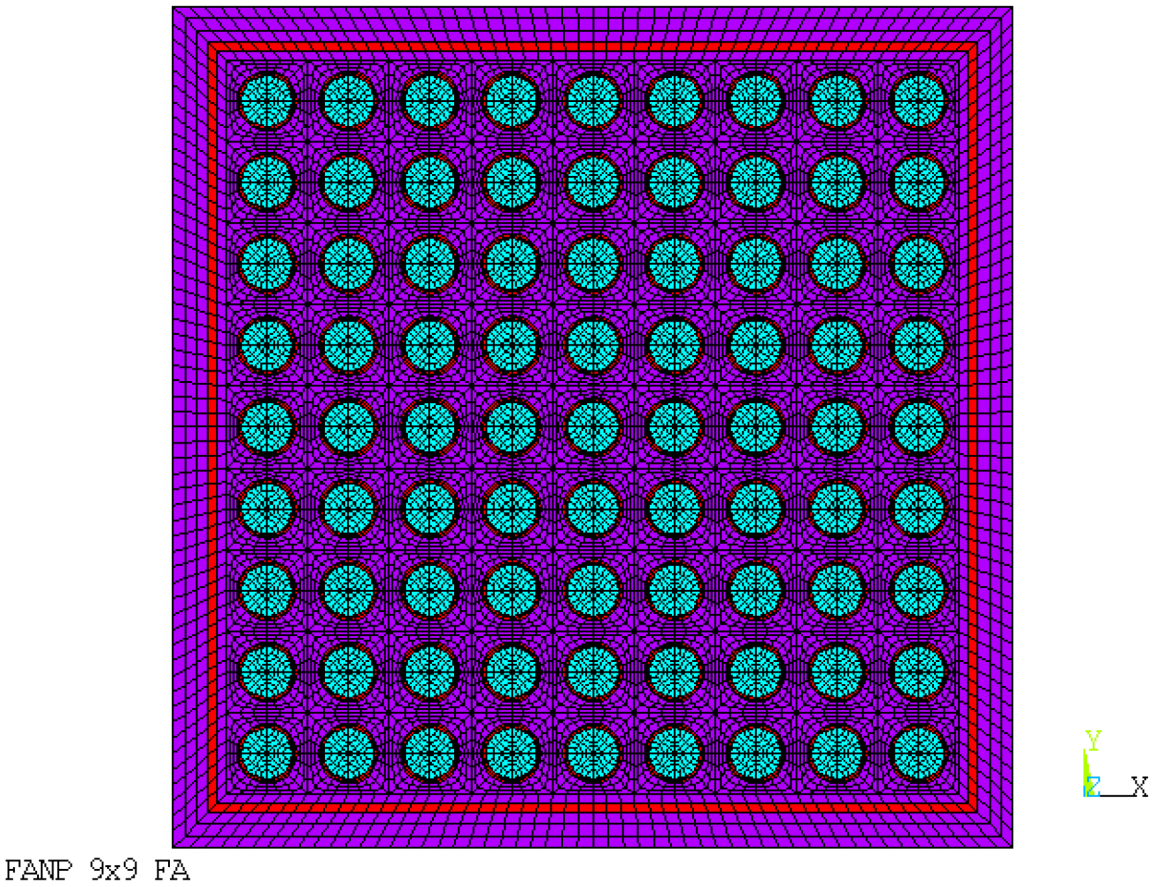

Figure 4.9.1-3
Finite Element Model of the FANP 9x9 Fuel Assembly

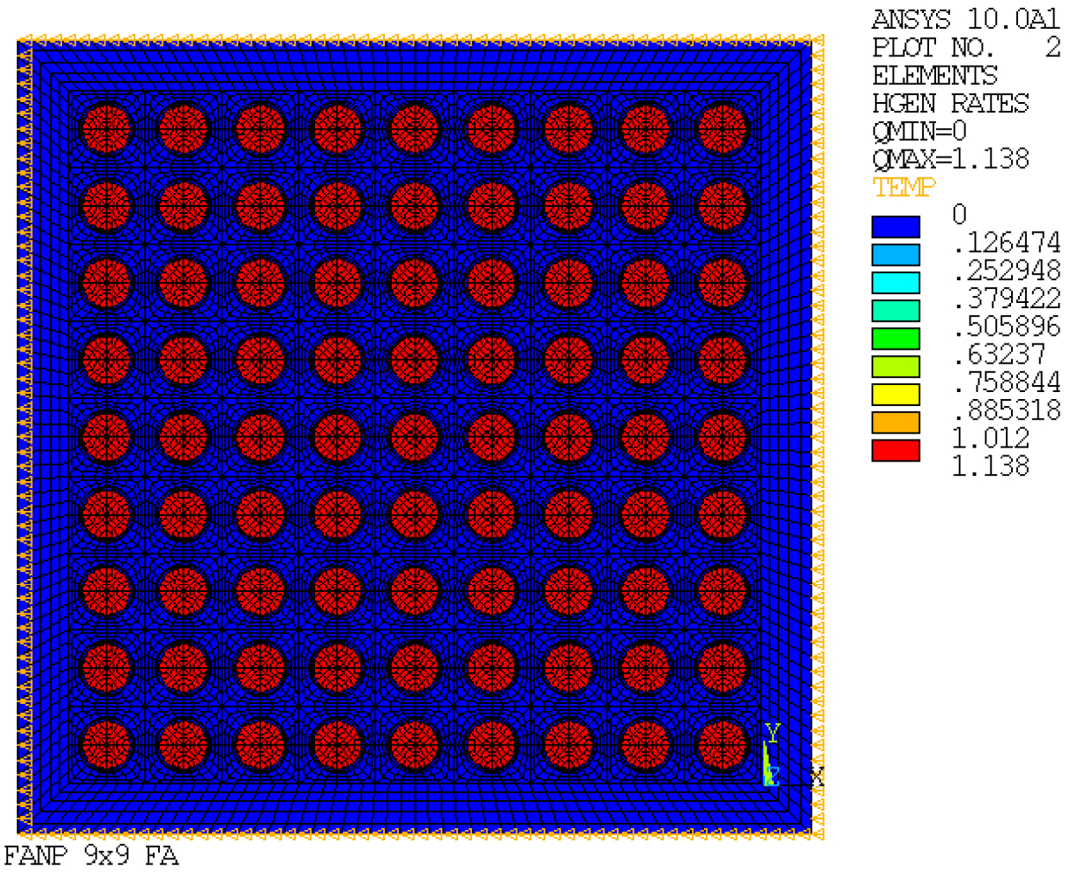

Figure 4.9.1-4
Heat Generation Rate and Temperature Boundary Conditions for FANP 9 x 9 Fuel Assemblies

Proprietary Information on Pages 4.9.2-i through 4.9.2-iii and 4.9.2-1 through 4.9.2-39
Withheld Pursuant to 10 CFR 2.390

APPENDIX 4.9.3
MESH SENSITIVITY

Table of Contents

List of Tables

List of Figures

4.9.3 MESH SENSITIVITY

4.9.3.1 Mesh Sensitivity for Storage Analysis

A grid convergence study of the ANSYS FLUENT computational fluid dynamics (CFD) model for the EOS horizontal storage module (HSM) loaded with the EOS-37PTH dry shielded canister (DSC) is performed to determine the discretization error of the solution. The discretization error is determined by using the five-step procedure for uncertainty estimation specified in Appendix A.4 of NUREG 2152 [4.9.3-8] based on Richardson extrapolation. The Richardson extrapolation method is currently the most robust method available for prediction of numerical uncertainty as noted in [4.9.3-8]. The five-step procedure specified in [4.9.3-8] is identical to the approach presented in Section 2-4.1 of American Society of Mechanical Engineers Standard for Verification and Validation in Computational Fluid Dynamics and Heat Transfer (ASME V&V) 20-2009 [4.9.3-1]. In addition to the discretization error, this section computes the observed order of accuracy (p) and compares it to the theoretical order of accuracy of the ANSYS FLUENT solution. Four grids are considered for the study of the ANSYS FLUENT model.

Proprietary Information on Pages 4.9.3-2 through 4.9.3-18
Withheld Pursuant to 10 CFR 2.390

4.9.3.3 References

4.9.3-1 American Society of Mechanical Engineers, "Standard for Verification and Validation in Computational Fluid Dynamics and Heat Transfer," ASME V&V 20-2009, November 30th, 2009.

4.9.3-2 ANSYS FLUENT, Version 14.0, ANSYS, Inc.

4.9.3-3 Ismail B. Celik et.al, "Procedure for Estimation and Reporting of Uncertainty Due to Discretization in CFD Applications," Journal of Fluids Engineering, ASME, July 2008, Volume 130.

4.9.3-4 Examining Spatial (Grid) Convergence, NPARC Alliance CFD Verification and Validation Website, http://www.grc.nasa.gov/WWW/wind/valid/tutorial/spatconv.html

4.9.3-5 NUREG-1536, Revision 1, "Standard Review Plan for Spent Fuel Dry Cask Storage Systems at a General License Facility," U.S. Nuclear Regulatory Commission, Office of Nuclear Material Safety and Safeguards.

4.9.3-6 Not used.

4.9.3-7 Not used.

4.9.3-8 U.S. NRC, Office of Nuclear Material Safety and Safeguards, "Computational Fluid Dynamics Best Practice Guidelines for Dry Cask Applications-Final Report," NUREG-2152, Rev. 0, March 2013.

Proprietary Information on Pages 4.9.3-20 through 4.9.3-23
Withheld Pursuant to 10 CFR 2.390

APPENDIX 4.9.4
WIND IMPACT ON THE THERMAL PERFORMANCE OF THE EOS-HSM

Table of Contents

List of Tables

List of Figures

Proprietary Information on Pages 4.9.4-1 through 4.9.4-10
Withheld Pursuant to 10 CFR 2.390

[

]

Among the different load cases evaluated for the EOS-HSM, [ ] results in the maximum air temperature rise of 138°F. The maximum air temperature rise is determined as the difference in the average air temperature between the inlet and outlet.

In summary, if the heat load of a DSC during storage operations is greater than 41.8 kW and less than or equal to 50 kW, wind deflectors will be implemented to ensure the thermal performance of the EOS-HSM remains within its allowable limits. For heat loads less than or equal to 41.8 kW, wind deflectors are not needed for EOS-37PTH DSC.

Further, for each HLZC (1 through 3), the maximum heat loads of the EOS-89BTH DSC are lower compared to the EOS-37PTH DSC. Therefore, the same restriction is also applicable for the EOS-89BTH DSCs. If the heat load of an EOS-89BTH during storage operations is greater than 41.6 kW and less than or equal to 43.6 kW, wind deflectors will be implemented to provide assurance that the thermal performance of the EOS-HSM remains within its allowable limits. For heat loads less than or equal to 41.6 kW, wind deflectors are not needed for the EOS-89BTH DSC.

In addition, wind deflectors are not necessary during accident conditions to maintain the maximum fuel cladding temperature below the allowable limit of 1058 °F. Based on the description presented in Section 4.4.1 for Load Case #5, the blocked vent accident condition considers a complete blockage of the inlet and outlet vents for 40-hour duration. Any loss or damage to the wind deflectors only affects the outlet vents. Therefore, the complete blockage of both the inlet and outlet vents as considered for the blocked vent accident condition bounds the loss of wind deflector accident condition.

Proprietary Information on Pages 4.9.4-12 through 4.9.4-16
Withheld Pursuant to 10 CFR 2.390

4.9.4.9 References

4.9.4-1 NUREG-2174, "Impact of Variation in Environmental Conditions on the Thermal Performance of Dry Storage Casks," U.S. NRC, Office of Nuclear Material Safety and Safeguards, Feb. 2015.

4.9.4-2 ANSYS ICEM CFD, Version 14.0, ANSYS, Inc.

4.9.4-3 ANSYS FLUENT, ANSYS FLUENT User's Guide, *ANSYS FLUENT Theory Guide,* Version 14.0, ANSYS, Inc.

4.9.4-4 Proposed CoC 1042 Appendix A, NUHOMS® EOS System Generic Technical Specifications, Amendment 0.

4.9.4-5 American Society of Mechanical Engineers, "Standard for Verification and Validation in Computational Fluid Dynamics and Heat Transfer," ASME V&V 20-2009, November 30th, 2009.

4.9.4-6 U.S. NRC, Office of Nuclear Material Safety and Safeguards, "Computational Fluid Dynamics Best Practice Guidelines for Dry Cask Applications-Final Report," NUREG-2152, Rev. 0, March 2013.

4.9.4-7 [

]

Table 4.9.4-1
Design Load Cases for Wind Effect Study of the EOS-HSM Loaded with EOS-37PTH DSC with Normal Hot Condition

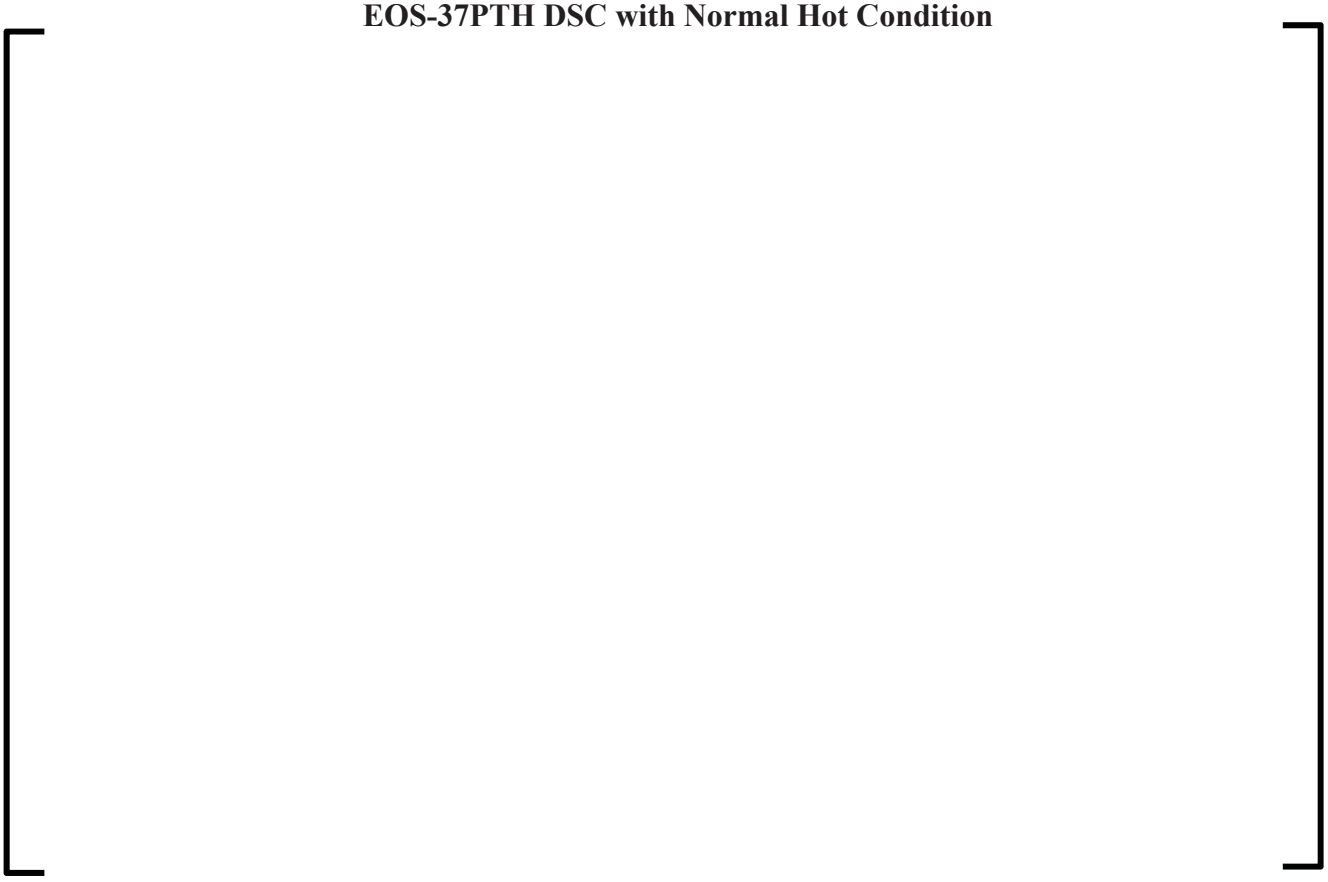

Table 4.9.4-2
Fuel Cladding and DSC Shell Temperatures

Load Case # (1)	DSC Shell Temperature (°F)		Maximum Fuel Cladding Temperature (°F)
	Maximum	Average	
1	422	352	724 (See Table 4-5)
F-1	406	336	< 724
F-2	397	323	< 724
F-3	388	296	< 724
B-1	417	349	< 724
B-2	416	345	< 724
B-3	406	335	< 724
S-1	434	361	< 735
S-2	436	366	735
	427 (2)	348 (2)	729 (2)
	409 (4)	330 (4)	713 (4)
S-3	430	362	< 735
2(3)	417	350	688

Notes:

(1) See Table 4.9.4-1 for the description of the load cases.

[

]

(4) These temperatures are determined based on a yearly average ambient temperature of 70 °F based on the discussion in Section 4.9.4.6.1.

Proprietary Information on Pages 4.9.4-20 through 4.9.4-39
Withheld Pursuant to 10 CFR 2.390